Check for updates

The spirobichroman-based polyimides with different side groups: from structure–property relationships to chain packing and gas transport performance†

Shuli Wang,[a] Xiaohua Tong,[a] Chunbo Wang,[a] Xiaocui Han,[a] Sizhuo Jin,[a] Daming Wang, [ID] *[a] Jianan Yao*[b] and Chunhai Chen [ID] [a]

Spirobichroman-based polymers with high gas permeability and selectivity are promising for their applications as membranes in gas separation. In this study, three spirobichroman-based polyimides (PIs; **6FDA-FH**, **6FDA-DH**, and **6FDA-MH**) were synthesised by the polyreaction between diamines containing different substituents (benzene ring, pyridine ring, and methyl group) and 4,4′-(hexafluoroisopropylidene)-diphthalic anhydride (6FDA). The physical properties, gas transport behaviour, d-spacing, dihedral angle of molecules, and fractional free volume of the PIs were investigated through experiments and molecular simulations. The PIs exhibited excellent thermal stability and good solubility in common organic solvents. The gas permeability of the PIs was investigated; the results highlighted the critical role of the substituents in the enhancement of the gas separation performance of polymer membranes. Detailed analysis of the PIs showed that **6FDA-FH** exhibits the highest gas permeability. This can be ascribed to the loose packing of the polymer chain owing to the increased dihedral angle between the two planes. However, the methyl substituent in **6FDA-MH** disrupts the polymer chain packing rather than changing the dihedral angle between the two planes, thus enhancing the gas permeability of **6FDA-MH**. Furthermore, **6FDA-DH** exhibited the highest CO_2/CH_4 selectivity, which is attributed to the CO_2 affinity of the polymer containing the pyridine unit.

1. Introduction

Since the concept of membrane separation was first proposed by Graham in 1866,[1] membrane separation technologies have been rapidly developed and are widely used in the field of gas separation for various purposes such as removal of acidic gas from natural gas, separation and recovery of hydrogen during the pyrolysis of petroleum, and enrichment of oxygen and nitrogen in the air.[2,3] Although numerous polymer membranes have been studied for their gas separation properties, fewer than 10 membranes have been used on a commercial scale.[4] One of the serious challenges that limits the wide-scale application of polymer membranes is the trade-off relationship between their gas permeability (gas throughput) and selectivity

(separation efficiency), which is illustrated by the empirical criterion of the Robeson upper bound.[5,6] This challenge arises because of the inadequate free volume of polymer and random size distribution of micropores. Hence, design of a molecular structure with a high free volume distribution and reduced chain mobility can effectively overcome the above-mentioned challenge.[7,8] Typically, the approach to tuning molecular structures focuses on two molecular design strategies: (i) incorporation of various twisted sites (*e.g.*, ethanoanthracene, spirobisindane, spirobifluorene, and triptycene units and Tröger's base) into the polymer skeleton to create intrinsic microporosity and allow for high free volume and appropriate size distribution and (ii) integration of bulky pendant groups into the polymer chain to facilitate the disruption of polymer chain packing and increase the free volume of the polymer.[9–12] For example, Filiz *et al.*[13] developed a series of *ortho*-allyloxy polyimides (PIs) with different ratios of allylation units. Their results showed that the fractional free volume (FFV) was improved by increasing the number of allyl ether sidechains.

In addition, a class of polymers of intrinsic microporosity (PIMs) was studied for verifying their applicability as a gas separation membrane. The main chain of these polymers contains a twisted spiro-centre (two rings that share one carbon

[a]National & Local Joint Engineering Laboratory for Synthesis Technology of High Performance Polymer, Key Laboratory of High Performance Plastics, Ministry of Education, College of Chemistry, Jilin University, Changchun 130012, China. E-mail: wangdaming@jlu.edu.cn

[b]Center for Advanced Low-Dimension Materials, State Key Laboratory for Modification of Chemical Fibers and Polymer Materials, College of Materials Science and Engineering, Donghua University, Shanghai 201600, China. E-mail: yjn@dhu.edu.cn

† Electronic supplementary information (ESI) available. See DOI: 10.1039/d0ra10113c

atom) and rigid rings in the form of dioxane units, which limit the free rotation of molecules, leading to ultrahigh free volume and appropriate distribution of free volume elements as well as excellent gas permeability and high selectivity.[14] For example, the ladder-type PIMs prepared by the post-treatment of PIM-1 with thioamide, tetrazole, and carboxyl, which exhibited excellent gas permeability and high gas pair selectivity.[15,16]

Despite the advantageous properties of PIMs as membranes for gas separations, the commercially application of PIs with high thermal stability and good mechanical properties is limited by the poor gas permeability of PIs.[17,18] Hence, the combination of PIMs with twisted spiro-centres and PIs to obtain PIM-PIs with excellent gas permeability has attracted widespread interest. This concept is realised by the introduction of a twisted spiro-centre into a skeleton of PI chains, leading to reduced flexibility and tight packing of the molecular chains, thereby increasing the free volume within the polymer membrane.[19] Moreover, the PIM-PIs containing two main components (diamine and dianhydride) can be used to independently adjust the properties of the polymers by changing the structure of the diamine and/or dianhydride monomer. These advantages have inspired researchers to focus on PIM-PIs or PIM-PIs with functional groups to improve the applicability of these polymers as membranes for gas separation. In particular, contorted 6FDA is one of the most suitable anhydride units for manufacturing PIM-PI membranes; thus, it can be used to produce semi-ladder PIs that can serve as membranes that can exhibit excellent gas separation performance.[20,21] For example, Li et al.[22] reported three 6FDA-based semi-ladder PIM-PIs that were prepared from spirobichroman-based diamines with different substituents and 6FDA dianhydride units. The results showed that these PI membranes have significantly higher gas permeability than commercially available polymers, including Kapton, Matrimid 5218, polycarbonate, polysulfone, and cellulose acetate.

Despite the high membrane performance of semi-ladder PIs, membranes with higher gas permeability and gas pair selectivity are required for improved gas separation. Hernandez et al.[23] fabricated a series of blend membranes based on 6FDA–6FpDA PIs and copolyfluorenes. Compared with the pure PI membrane, their blend membranes exhibited higher CO_2 permeability and CO_2/CH_4 selectivity (>23% and 15%, respectively) when the content of polyfluorene was approximately 1%. In addition, many semi-ladder PIs with functional groups have been developed to improve the capacity of their interactions with different gases. Tena et al.[24] successfully obtained functionalised polymers by the 3,3'-sigmatropic Claisen rearrangement, indicating that the incorporation of specific functional groups in the polymer backbone can enhance the performance of the materials. The tertiary amine of the pyridine unit integrated into the polymer was expected to be responsible for the increase in CO_2 affinity of the polymer, which was anticipated to enhance CO_2 selectivity and permeability toward other slow gases such as CH_4 or N_2.[25] Wang et al.[26] prepared PIM-PIs by functionalisation with a tertiary amine, and the resultant polymer membrane offered high gas permeability and improved gas pair selectivity for CO_2/CH_4 and CO_2/N_2, owing to the enhanced

solubility of CO_2 as a result of the interaction between tertiary amines and CO_2.

Based on the findings of the above-mentioned studies, we developed new semi-ladder PIM-PIs containing functional groups consisting of pyridine units in this study. Furthermore, the structure–property relationships of the new PIM-PIs were investigated by combining experimental data and molecular simulations, with the aim of expanding their application as membranes for gas separation. Herein, we designed and synthesised three spirobichroman-based PIs (**6FDA-FH**, **6FDA-DH**, and **6FDA-MH**) through a series of reactions with 4,4,4',4'-tetramethyl-2,2'-spirobi[chromane]-7,7'-diol (Spiro-diol; Fig. 1) and 6FDA. We expected that the integration of both the contorted spirobichroman-based unit and the functional side group into the PIM-PIs will disrupt the packing of polymer chains and enhance the overall separation performance of PIs. Finally, the effects of the substituents on chain packing and gas transport were investigated in detail.

2. Experimental section

2.1. Reagents and methods

Resorcinol (99%), mesityl oxide (95%), iron chloride (>99.99%, $FeCl_3$), 4-chloronitrobenzene (98%), 2-chloro-5-nitropyridine (98%), 2-chloro-3-methyl-5-nitropyridine (99%), potassium carbonate (>99%, K_2CO_3), Pd/C (10%), and hydrazine monohydrate ($N_2H_4 \cdot H_2O$, 85%) were purchased from Aladdin and used as received. 4,4'-(Hexafluoroisopropylidene)-diphthalic anhydride (6FDA, 99%) was acquired from TCI and sublimated in vacuum before use. Toluene, N,N-dimethylacetamide (DMAc), and N,N-dimethylformamide (DMF) were dried using 4 Å molecular sieves.

Nuclear magnetic resonance (NMR) spectroscopy was conducted on a BRUKER-300 spectrometer with deuterated dimethyl sulfone as the solvent. Fourier transform infrared (FTIR) spectroscopy was performed on a Bruker Vector 22 spectrometer. Gel permeation chromatography (GPC, PL-GPC 220) was carried out by using polystyrene as the standard and
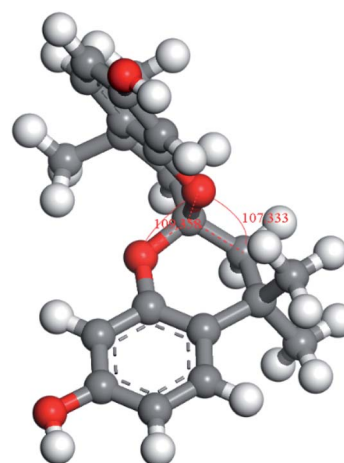

Fig. 1 Energy-minimised conformation of spirobichroman-based diphenol.

DMF as the eluent to determine the molecular weight of the polymer. Differential scanning calorimetry (DSC, TA Q100) was performed to evaluate the glass transition temperature (T_g) of the polymer at a heating rate of 10 °C·min^{-1}, and the T_g value was calculated after the second heating cycle. Thermogravimetric analysis (TGA, TA 2050) was carried out at a heating rate of 10 °C min^{-1} under nitrogen and air atmospheres, respectively. Wide-angle X-ray diffraction (WAXD) analysis was conducted on a Bruker D-8 Advance diffractometer with Cu Kα radiation. The *d*-spacing of the polymer was determined using Bragg's law ($d = \lambda/2 \sin\theta$, $\lambda = 1.54$ Å).

The density (ρ) of the polymer was measured using sophisticated electronic balance equipment by the buoyancy method in deionised water at 25 °C. The FFV of the polymer was calculated using eqn (1)–(3):[27]

$$V_0 = 1.3 V_w \quad (1)$$

$$V = \frac{M}{\rho} \quad (2)$$

$$V_f = \frac{V - V_0}{V} \quad (3)$$

Here, V_w derived from Bondi's group contribution theory, is the specific van der Waals volume, M (g mol^{-1}) is the molar mass from the repeat unit of the polymer, V (cm^3 mol^{-1}) is the molar volume of the polymer, and V_f is the FFV of the polymer.

The permeability of pure gases (*e.g.*, O$_2$, N$_2$, CO$_2$, and CH$_4$) was measured by the constant-volume method at 2 barrer and 35 °C. Gas permeability (P) and selectivity ($\alpha_{A/B}$) are calculated according to eqn (4) and (5), respectively.[28]

$$P = DS = \frac{273}{76} \frac{Vl}{ATP_0} \frac{dp(t)}{dt} \quad (4)$$

$$\alpha_{A/B} = \frac{P_A}{P_B} = \frac{D_A}{D_B} \times \frac{S_A}{S_B} = \alpha_{A/B}^D \times \alpha_{A/B}^S \quad (5)$$

Here, V (cm^3) is the downstream chamber volume, A (cm^2) and l (cm) are the effective area and thickness of the membrane, respectively; T (K) is the trial temperature of the experiment; P_0 (cmHg) is the upstream pressure of the instrument; and dp/dt is the rate at which the pressure changes during the experiment D and S are the diffusion and solubility coefficients, respectively. $\alpha_{A/B}$ is the ideal selectivity coefficient of the gas, which is derived from the diffusion selectivity ($\alpha_{A/B}^D$) and solubility selectivity ($\alpha_{A/B}^S$).

The FFVs of the polymer were calculated using Materials Studio 2017. First, an amorphous cell containing 15 repeat units was established as the initial model, and the density of the polymer cell was set to 0.01 g cm^{-3}. Then, the cell of the polymer was compressed by the normal pressure and temperature (NPT) ensemble until the density approached the measured value. The simulation step size and time for the NPT ensemble were 1 fs and 100 ps, respectively. The structure of the polymer was then balanced by the normal volume and temperature ensemble, and the equilibration time and step size were 100 ps and 1 fs, respectively. The dynamics simulation was performed using the

universal force field. Once the balanced state of the polymer was achieved, the simulation was continued.[29]

Furthermore, the dihedral angle of the two adjacent planes was calculated using Materials Studio 2017. The dihedral angles were incrementally varied from −180° to +180° using the Conformers module. Energy minimisations of all conformers were conducted on the Forcite module by the COMPASS force field. Then, the torsional degree of freedom was estimated when the thermal energy was close to 3 RT.[30]
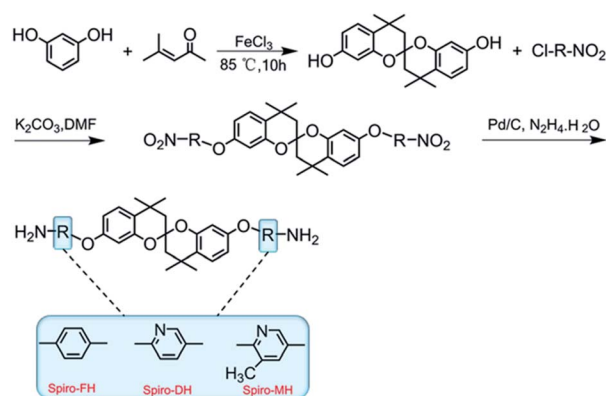
2.2. Membrane preparation

The membrane (60–70 μm) was prepared by the solution casting method. Specifically, the polymer was dissolved in chloroform (w/w = 5–8%) and filtered using a 4.5 μm filter to remove any insoluble material. The filtrate was carefully poured into a clean glass Petri dish and placed in a sealed device; then, the solvent was evaporated at 25 °C for 3 days. Finally, the membrane was heated in vacuum at 120 °C for 12 h to remove the residual solvent.

2.3. Monomer synthesis

2.3.1 Synthesis of 4,4,4′,4′-tetramethyl-2,2′-spirobi[chromane]-7,7′-diol (Spiro-diol). Spiro-diol was obtained according to a previously reported method,[31] as shown in Scheme 1. Details of the synthesis process are provided in the experimental section of the ESI.†

2.3.2 Synthesis of spirobichroman-based dinitro monomers. The dinitro monomers, Spiro-FN, Spiro-DN, and Spiro-MN were synthesised by a nucleophilic substitution reaction using the appropriate reagents; the synthetic route is shown in Scheme 1. The specific synthesis process of 4,4,4′,4′-tetramethyl-7,7′-bis(4-nitrophenoxy)-2,2′-spirobi[chromane] (Spiro-FN) is used as an example and is presented in the experimental section of the ESI.†

2.3.3 Synthesis of spirobichroman-based diamine monomers. The diamine monomers (**Spiro-FH**, **Spiro-DH**, and **Spiro-MH**) were obtained by a reduction reaction, using Pd/C and N$_2$H$_4$·H$_2$O as the catalyst and reductant, respectively. The synthetic process of the diamine monomer was explained using 4,4′-((4,4,4′,4′-tetramethyl-2,2′-spirobi[chromane]-7,7′-diyl)

Scheme 1 Synthetic routes to **Spiro-FH**, **Spiro-DH**, and **Spiro-MH**.

bis(oxy))dianiline (**Spiro-FH**) as an example, as shown in the experimental section of the ESI.†

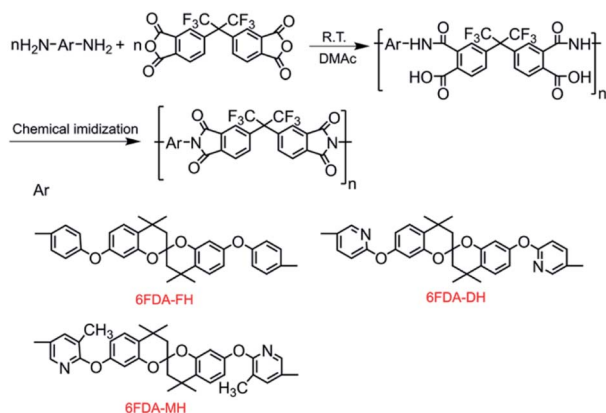### 2.4. Synthesis of spirobichroman-based PIs

The PIs (**6FDA-FH**, **6FDA-DH**, and **6FAD-MH**) were synthesised by chemical imidisation, as shown in Scheme 2. The preparation of **6FDA-FH** serves as an example to illustrate the detailed synthesis process and is presented in the experimental section of the ESI.†

3. Results and discussion

3.1. Synthesis and characterisation of spirobichroman-based monomers and PIs

The diamine monomers were synthesised through a multistep reaction process, as shown in Scheme 1. From the FTIR and NMR spectra, the chemical structure of the three monomers was confirmed. As depicted in Fig. S1 (ESI†), the $-NO_2$ absorption peaks at 1509–1523 cm^{-1} and 1342–1355 cm^{-1} disappeared, and the N–H stretching band of amine appeared at 3426–3473 cm^{-1}. The ^{1}H NMR and ^{13}C NMR spectra of the diamine monomers are shown in Fig. S2 and S3, respectively (ESI†). All the resonance signals were appropriately assigned to the chemical structure of these molecules. These results confirmed that the diamine monomers were successfully synthesised. Theoretically, the chemical shifts of the $-CH_3$ groups at the spiro-centres on the diamine monomers should be the same because they are in the same chemical environment. However, the bulky $-CH_3$ groups to the sides of the spiro-centre limit the rotation of the molecules, resulting in the formation of chiro isomers.[22] In addition, the chemical shifts of the amine protons in **Spiro-FH**, **Spiro-DH**, and **Spiro-MH** are 4.97, 5.09, and 5.02 ppm, respectively. Compared with the amine proton at 4.97 ppm in **Spiro-FH**, the amine protons in **Spiro-DH** and **Spiro-MH** are shifted downfield. This is because the pyridine unit in the **Spiro-DH** and **Spiro-MH** contains lone-pair electrons, resulting in a strong electron-withdrawing effect.

Spirobichroman-based PIs (**6FDA-FH**, **6FDA-DH**, and **6FDA-MH**) were successfully synthesised by reacting 6FDA with the corresponding diamines *via* chemical imidisation (Scheme 2).

Scheme 2 Synthetic routes to **6FDA-FH**, **6FDA-DH**, and **6FDA-MH**.

The chemical structure of the PIs was confirmed by FTIR and ^{1}H NMR spectroscopy. As shown in Fig. S4 (ESI†), the representative characteristic peaks of the imide group were observed at 1780–1785 cm^{-1} (C=O symmetric stretching) and 1728–1738 cm^{-1} (C=O asymmetric stretching). The peak ascribed to N–H bending was observed at 1375–1388 cm^{-1}. The ^{1}H NMR spectrum of the PIs is shown in Fig. S5 (ESI†). All chemical shifts of the protons on the ^{1}H NMR spectrum of the polymer repeat unit were satisfactorily assigned, and the integral values corresponded to the chemical structure of the polymer. The intrinsic physical behaviour of the PIs was investigated in detail by determining the molecular weights of the three polymers (Table 1). The polymers exhibited high molecular weights ($M_n = 7.7$–17.2×10^4) and narrow molecular weight distribution (PDI = 1.14–1.79), which is beneficial for the processing technology of the membrane. The molecular weights of the polymers decreased in the order **6FDA-FH** > **6FDA-DH** > **6FDA-MH**; this decrease can be primarily attributed to the reactivity of the diamine moiety.[32] As shown in Fig. 2, the net charges of the N atom of the amine unit decrease in the following order: **Spiro-FH** > **Spiro-MH** > **Spiro-DH**. Therefore, **Spiro-FH** has the highest nucleophilicity among the three diamines and can be used to obtain the longest PI molecular chain.[22] Although the nucleophilicity of **Spiro-DH** is lower than that of **6FDA-MH**, the high molecular weight of **6FDA-DH**, which is higher than that of **6FDA-MH**, could be attributed to the low polarity of the amine of **Spiro-MH** when $-CH_3$ is present at the *meta*-position of amine. The relatively low polarity effect weakens the reactivity of the diamine moiety to the dianhydride monomer and results in the formation of the polymer with a relatively low molecular weight.[21]

3.2. Thermal properties of PIs

The thermal behaviour of the PIs was investigated by DSC and TGA; the T_g results are shown in Fig. 3 and Table 1. The results confirm that all PIs have an amorphous structure.[33] The T_g of the polymers ranges from 270 to 278 °C in the order **6FDA-DH** > **6FDA-FH** > **6FDA-MH**. According to Flory's theory, the factors influencing the T_g of polymers are the rigidity of the polymer molecular chains and the interactions.[34] In this regard, **6FDA-MH** has a bulky substituent in the form of the $-CH_3$ group, which increases the flexibility of the polymer chain. Hence, the T_g of **6FDA-MH** is the lowest among the three polymers, whereas **6FDA-DH** had the highest T_g, which is attributed to the strongest interactions between the molecular chains in all synthesised polymers.[35]

The thermostability of the polymers under N$_2$ and air atmospheres is shown in Fig. 4 and S6 (ESI†), respectively, and the specific results are summarised in Table 1. The thermal decomposition temperature of the polymers at 5% weight loss was 438–469 °C and 435–466 °C in N$_2$ and air, respectively. The residual weight of the polymers was observed to be 41–47% at 800 °C. These results demonstrate that the polymers exhibit good thermal stability. Nevertheless, the thermal decomposition temperature at 5% weight loss is the lowest for **6FDA-MH**, which is attributed to the presence of an aliphatic structure,

Table 1 Thermal properties and molecular weights of the polyimides

	$T_g{}^a$ (°C)	$T_{5\%}{}^b$ (°C)		$T_{10\%}{}^b$ (°C)		Molecular weights^c			
Polymer	DSC	N$_2$	Air	N$_2$	Air	$R_w\%^d$	M_n	M_w	PDI (M_w/M_n)
6FDA-FH	273	469	466	481	482	41	17.2×10^4	30.8×10^4	1.79
6FDA-DH	278	446	440	460	461	47	8.1×10^4	11.7×10^4	1.44
6FDA-MH	270	438	435	451	456	46	7.7×10^4	8.9×10^4	1.14

^{a} T_g was determined by DSC. ^{b} The thermal decomposition temperatures at 5% and 10% weight loss were determined by TGA. ^{c} Molecular weights were obtained using GPC. ^{d} Residual rates at 800 °C were recorded by TGA under N$_2$ atmosphere.
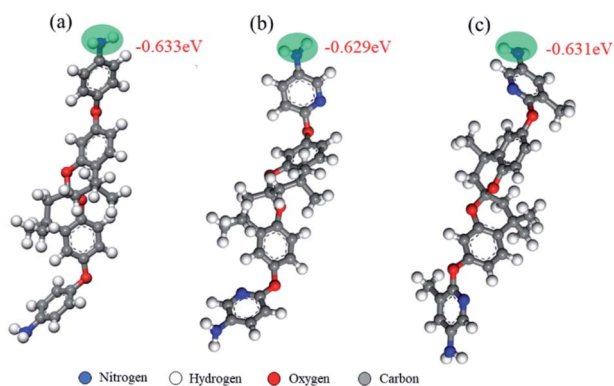

Fig. 2 Net charges of the nitrogen atom in the amine units calculated by Materials Studio 2017. (a), (b), and (c) represent **Spiro-FH**, **Spiro-DH**, and **Spiro-MH**, respectively.
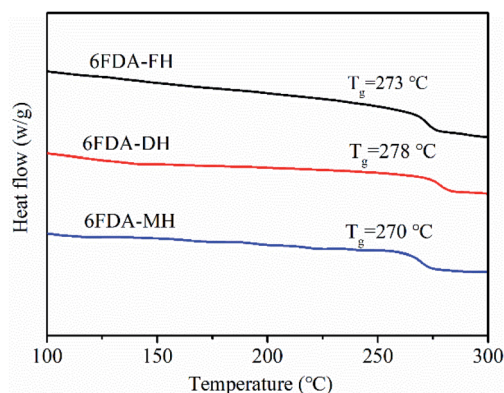

Fig. 4 TGA curves of the three PIs under N$_2$.

Fig. 3 DSC curves of the three PIs.

namely, the –CH$_3$ group.[36] In addition, owing to the higher aromaticity of the phenyl ring compared with that of the pyridyl ring, at 5% weight loss, the thermal stability of **6FDA-FH** is higher than that of **6FDA-DH**.

3.3. Solubility and morphology of PIs

Owing to the strong interaction between the intermolecular chain and the rigid structure of the imine ring, aromatic PIs are typically poorly soluble in common organic solvents. Thus, optimisation of polymer performance is necessitated. And the
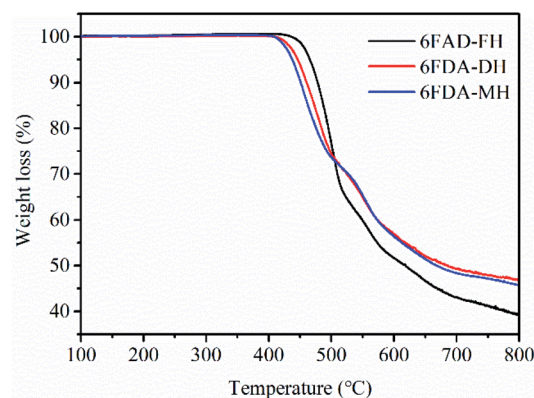
relationship between the spirobichroman-based polymers and solubility was studied; the results are summarised in Table 2. The three PIs exhibited excellent solubility in common organic solvents, including chloroform and tetrahydrofuran that have low boiling points. Following are the reasons for the high solubility of the polymer: (i) the spirobichroman-based structure and the presence of large bulky –C(CF$_3$)$_2$– groups increased the noncoplanarity of the molecule and reduced the density of the polymer packing; (ii) an electron-deficient heterocyclic pyridine unit was incorporated into the polymer, enhancing the dipole–dipole interaction between the polymer and solvent, thus increasing polymer solubility; and (iii) the ether bond is considered to increase the movement of chain segments and enhance the solubility of the polymer in organic solvents.[37–39]

Furthermore, the morphology of the synthesised PIs was investigated through WAXD analysis. The results are shown in Fig. 5, and the corresponding values measured for the chain spacing (d-spacing) are listed in Table 3. All polymers had a broad diffraction peak, confirming the amorphous morphology of the polymers in correspondence with the DSC measurements.[40] The d-spacing of the polymers decreased in the order **6FDA-FH** > **6FDA-MH** > **6FDA-DH**, because of the presence of different substituents of the polymers. The dihedral angles between the substituent and the plane of the adjacent benzene ring were determined; these angles are denoted as α_1, α_2, and α_3 for **6FDA-FH**, **6FDA-DH**, and **6FDA-MH**, respectively. As shown in Fig. 6 and Table 3, α_2 and α_3 are smaller than α_1. This is because the substituted pyridine unit has higher polarity

Table 2 Solubility of the three PIs in common organic solvents

Polymer	Solubility[a]							
	DMAc	DMF	NMP	DMSO	THF	CHCl$_3$	1,4-Dioxane	Ethanol
6FDA-FH	+	+	+	+	+	+	+	−
6FDA-DH	+	+	+	+	+	+	+	−
6FDA-MH	+	+	+	+	+	+	+	−

[a] 10 mg polymer was dissolved in 1 mL organic solvent at room temperature for 24 h. + completely dissolved; − insoluble.
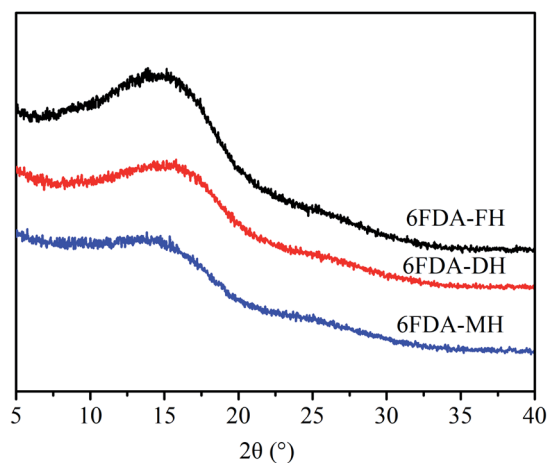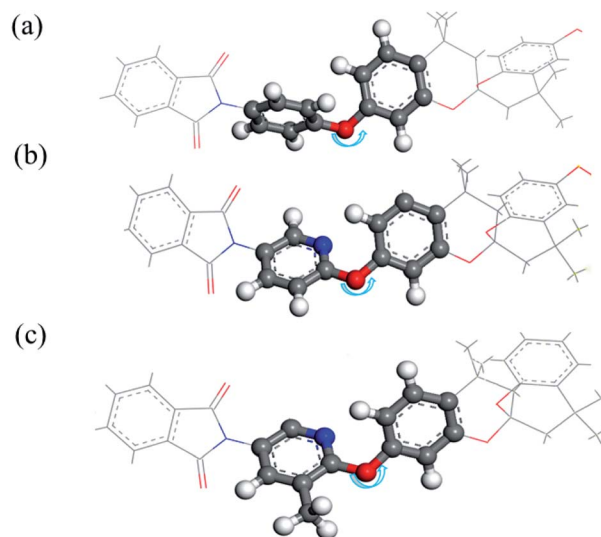
Fig. 5 WAXD patterns of the three PIs.

Fig. 6 Dihedral angles α_1 (a), α_2 (b), and α_3 (c) of **6FDA-FH**, **6FDA-DH**, and **6FDA-MH**, respectively.

than the benzene ring in **6FDA-DH** and **6FDA-MH**, thus affording a higher degree of coplanarity between the planes of the substituent and the adjacent benzene ring. Hence, the *d*-spacing of **6FDA-DH** and **6FDA-MH** was smaller than that of **6FDA-FH**. The dihedral angle between the plane of the pyridine ring and that of the adjacent benzene ring of **6FDA-DH** and **6FDA-MH** did not differ significantly, which confirmed that the –CH$_3$ substituent had a negligible effect on the dihedral angle of the two planes. However, the bulky –CH$_3$ substituent could disrupt the packing of the polymer chains, resulting in a larger *d*-spacing of **6FDA-MH** than that of **6FDA-DH**.

3.4. Fractional free volume (FFV) of the PIs

The free volume and free volume distribution of glassy polymers are known to affect gas permeability and selectivity. The FFVs of

the polymers, derived from the polymer density and molecular dynamics simulation, are listed in Table 3. The highest FFV value of **6FDA-FH** is attributable to the large dihedral angle between the plane of the benzene ring and that of the adjacent plane in **6FDA-FH**, which resulted in more loosely packed molecular chains. Furthermore, **6FDA-MH**, with the –CH$_3$ substituents, has higher FFV than **6FDA-DH**. This is because the –CH$_3$ group introduces additional steric hindrance and disrupts the packing of the polymer chain. In this regard, molecular dynamics simulation is considered an effective method to gain deep insight into the microporous structure and free volume distribution of glassy polymers.[32] As illustrated in Fig. 7, the

Table 3 Fraction free volume (FFV), chain spacing (*d*-spacing), and dihedral angle (α) of the three PIs

Polymer	ρ^a (g cm^{-3})	M (g mol^{-1})	$V_w{}^b$ (cm^3 mol^{-1})	FFV		d (Å)	α (°)
				Found	Simulated		
6FDA-FH	1.231	931	504.42	0.133	0.107	5.89	65
6FDA-DH	1.350	933	487.62	0.083	0.101	5.57	53
6FDA-MH	1.264	961	507.56	0.132	0.106	5.79	54

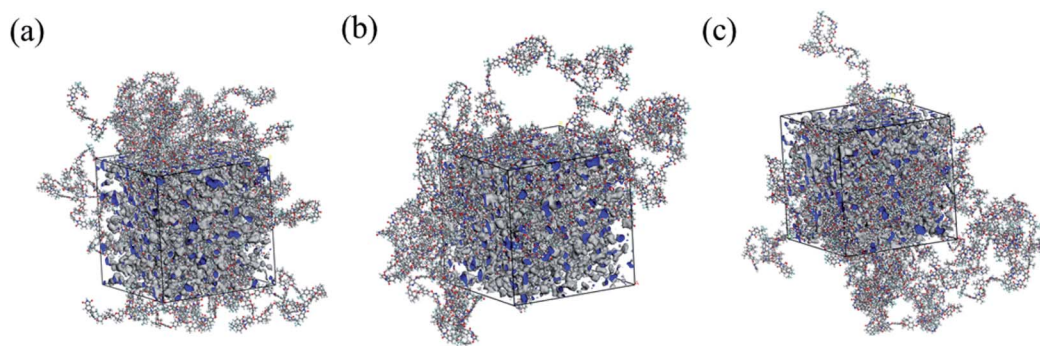[a] Density of the polymer. [b] Specific van der Waals volume.

Fig. 7 Three-dimensional view of the free volume distribution of the polymers calculated using Material Studio 2017. The images in (a), (b), and (c) represents **6FDA-FH**, **6FDA-DH**, and **6FDA-MH**, respectively.

grey and blue areas represent the ektexine of free space and cross-section of cut free space, respectively. The existence of three-dimensional continuous cavities proved the loose packing structure of the polymers.[41,42] Although the tendency of the FFVs is consistent with the experimental values and molecular dynamics simulation, the differences in the values obtained by the two methods are attributed to the following: (i) the multiple 1.3 molecular chain packing was reasonable in Bondi's group contribution method but not accepted in the actual molecular chain packing of glassy polymers; (ii) the semi-empirical formulas were used to optimise the force field in the process of simulation, resulting in an inherent error.[43–45]

3.5. Pure-gas transport for PI membranes

The permeability of pure gases (N_2, CH_4, O_2, and CO_2) and ideal selectivity of the three spirobichroman-based PI membranes are listed in Table 4. The three PI membranes produced high gas pair selectivity of $\alpha_{CO_2/CH_4} > 37$ and $\alpha_{CO_2/N_2} > 24$. The gas permeability of the membranes decreased in the order $P(CO_2) > P(O_2) > P(N_2) > P(CH_4)$, and the results demonstrated that the

order in which the gases permeate through the polymer membranes is consistent with that of the molecular kinetic diameters and followed the molecular sieve effect.[46] In particular, N_2 allows for a more obvious molecular sieve effect than CO_2 because of its relatively large molecular kinetic diameter.[32] Hence, the permeability of N_2 for all membranes is observed to be lower than that of CO_2. **6FDA-FH** exhibited the highest gas permeability among the three PI membranes, owing to its relatively large FFV and d-spacing, which improve gas passageways. Compared with the **6FDA-DH** membrane, the **6FDA-MH** membrane has higher gas permeability; this is because the $-CH_3$ substituent disrupts chain packing and increases the FFV of the polymer. This result indicates that the $-CH_3$ substituent could contribute to improve the gas permeability of the polymer membrane. In addition, although the **6FDA-DH** and **6FDA-MH** membranes contain the tertiary amine from pyridine units, the CO_2 permeability of these two membranes was lower than that of the **6FDA-FH** membrane. The reasons for the low permeability were as follows: the presence of tertiary amine groups from the pyridine unit in **6FDA-DH** and **6FDA-MH** leads to strong CO_2 adsorption, thereby resulting in a high CO_2 solubility coefficient (S) and improved CO_2 permeability.[26] However, the introduction of polarity unit pyridine ring into the polymer enhanced the coplanarity between the plane of the pyridine ring and that of the adjacent benzene ring and led to denser chain packing. Therefore, the FFVs of the **6FDA-DH** and **6FDA-MH** membranes were lower than that of the **6FDA-FH** membranes and reduced the CO_2 permeability performance. The results indicated that FFV of polymer exerts a greater effect on CO_2 permeability than the strong CO_2–polymer interaction.

Table 4 also lists the membrane gas transport properties of different types of PIs, which contain different diamine monomers and 6FDA dianhydride. Compared with XS1 and XS4, which have the binaphthyl structure, the FFVs of the three spirobichroman-based PIs were enhanced because of the presence of their twisted spirobichroman-based structure disrupts the chain packing, thereby improving gas permeability. It is noteworthy that the CO_2 permeability of **6FDA-FH** was 3.96 and 3.39 times higher than those of XS1 and XS4, respectively. These results indicate that the spirobichroman-based PI membranes

Table 4 Pure-gas permeability (P) and ideal selectivity (α) of the three PI membranes

Polymer	Permeability[a] (barrer)				Selectivity ($\alpha_{A/B}$)		
	N_2	CH_4	O_2	CO_2	CO_2/N_2	CO_2/CH_4	O_2/N_2
6FDA-FH	0.66	0.44	4.06	17.11	25.9	38.9	6.2
6FDA-DH	0.29	0.19	1.80	7.99	27.6	42.1	6.2
6FDA-MH	0.54	0.36	3.41	13.34	24.7	37.1	6.3
XS1 (ref. 48)	0.14	0.09	0.98	4.32	29.9	50.2	6.8
XS4 (ref. 48)	0.23	0.12	1.19	5.05	22.1	41.3	5.2
6FDA-MSBC[22]	1.42	0.77	5.55	21.2	—	27.6	3.92
6FDA-FSBC[22]	3.69	2.55	17.0	66.0	—	25.8	4.60
6FDA-SBC[22]	1.87	1.28	8.19	32.1	—	25.1	4.38
6FDA-OHB[47]	1.23	0.81	6.4	35	—	—	—
6FDA-6HpDA[47]	1.44	0.84	7.1	36	—	—	—
6FDA-6FpDA[47]	2.5	1.29	11.8	55	—	—	—
6FDA-OFB[47]	9.7	5.2	36	160	—	—	—
TB-PI[46]	10	6.3	50	190	—	30.2	5.0

[a] 1 barrer = 10^{-10} cm^3 (STP) cm cm^{-2} s^{-1} $cmHg^{-1}$.

hold potential as promising high-performance gas separation membrane materials. The gas permeability of the three PI membranes in the present work is lower than that of 6FDA-MSBC, 6FDA-FSBC, and 6FDA-SBC.[22] This low permeability can mainly be ascribed to the presence of the bulky methyl or aromatic fluoro-substituent in 6FDA-MSBC, 6FDA-FSBC, and 6FDA-SBC, which disrupts the chain packing and increases the FFV of the polymers. PI membranes based on 6FDA that contain rigid V-shape bridged bicyclic linking groups (*e.g.*, Tröger's base)[46,47] exhibit considerably higher gas permeability than the PI membrane with the spirobichroman-based structure. This phenomenon could be attributed to the fact that Tröger's base unit significantly disrupts chain packing, resulting in higher FFV than that of spirobichroman-based PIs. However, the selectivity of the gas pairs containing the rigid Tröger's base unit PI (TB-PI) is obviously lower than that of spirobichroman-based PIs (**6FDA-FH, 6FDA-DH,** and 6FDA-FSBC). This reveals that the introduction of the spirobichroman-based moieties into the **6FDA-FH, 6FDA-DH,** and 6FDA-FSBC backbones enhances microporosity and results in higher gas pair selectivity.[37]

To estimate the gas separation performance of the spirobichroman-based PI membranes, the trade-off relationship between gas permeability and selectivity for CO_2/CH_4 and O_2/N_2 was investigated using the Robeson upper bounds as references, as shown in Fig. 8. Polymer membranes with high gas pair selectivity are known to typically couple with low gas permeability. Obviously, this general trade-off relationship is applicable to the present work. The CO_2 permeability of **6FDA-DH** is lower than that of **6FAD-FH**, and this was accompanied by an increase in CO_2/CH_4 selectivity owing to the sharp decline in CH_4 permeability. Although the comprehensive separation performance of the membranes was lower than the Robeson upper bound, **6FDA-FH** exhibited the most promising gas separation performance among the three PI membranes. The excellent performance is attributed to the greatly enhanced gas permeability of **6FDA-FH** relative to that of **6FDA-DH** and **6FDA-MH**, and the **6FDA-FH** membrane maintains high gas pair selectivity. Compared with the reported PI membranes of XS1

and XS4,[48] the performance of the three spirobichroman-based PI membranes is overall higher in terms of the permeability/ selectivity trade-off for CO_2/CH_4 and O_2/N_2 gas pairs (see Fig. 8). The significant increase in FFV induced by the incorporation of spirobichroman-based units in PI markedly enhances the gas separation performance of the membranes compared with that of the PI membrane that contains a binaphthyl structure (XS1 and XS4). However, the comprehensive separation performance of the three spirobichroman-based PI membrane for the CO_2/CH_4 and O_2/N_2 gas pairs is lower than that of the reported polymers, which contain bulky substituting groups (6FDA-MSBC, 6FDA-FSBC and 6FDA-SBC) or possess rigidity arising from Tröger's base (TB-PI).[22,46] The results further highlight that the introduction of bulky side groups or rigid chain structures in the polymer promotes loose polymer chain packing and improves the comprehensive separation performance of gas pairs.

To understand the contribution of gas diffusivity (D) and solubility (S) to CO_2 and CH_4 transport behaviour in polymer membranes, the diffusivity and solubility of CO_2 and CH_4 were calculated by the time-lag method.[34] As displayed in Table 5, the diffusivity of gas in different polymer membranes decreases in the order **6FDA-FH** > **6FDA-MH** > **6FDA-DH**, which is consistent with the trends for FFV and d-spacing of the polymers (Table 3).

Table 5 Pure-gas (CO_2 and CH_4) diffusivity (D), solubility (S), diffusion selectivity (α_D), and solubility selectivity (α_S) of the three PI membranes

Polymer	D^a (10^{-9} cm^2 s^{-1})		S^b (10^{-2} cm^3 (STP) cm^{-3} cmHg^{-1})		α_D	α_S
	CO_2	CH_4	CO_2	CH_4	CO_2/CH_4	CO_2/CH_4
6FDA-FH	18.17	3.77	9.42	1.17	4.82	8.05
6FDA-DH	8.96	3.43	8.92	0.55	2.61	16.22
6FDA-MH	11.5	3.76	11.6	0.96	3.06	12.08

^{a} D was calculated by the time-lag method using $D = l^2/6\theta$ (l and θ are the membrane thickness and the lag time, respectively). ^{b} $S = P/D$ (P is the permeability of gas).
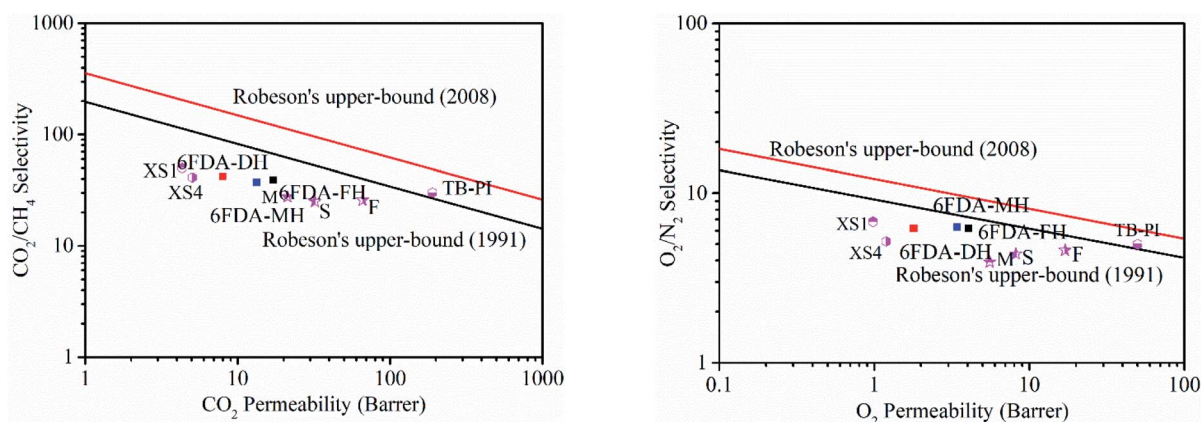

Fig. 8 Robeson's upper bounds relevant to the three PIs (**6FDA-FH, 6FDA-DH,** and **6FDA-MH**) for CO_2/CH_4 and O_2/N_2. The data points are those of XS1,[48] XS4,[48] M (6FDA-MSBC),[22] F (6FDA-FSBC),[22] S (6FDA-SBC),[22] and TB-PI.[46]

Compared with the CO_2 solubility and diffusivity of **6FDA-FH** and **6FDA-DH**, the CO_2 diffusivity of **6FDA-FH** is significantly higher than that of the **6FDA-DH**. This implies that the improvement of CO_2 permeability from **6FDA-DH** to **6FDA-FH** is mainly attributable to the increase in FFV, which is consistent with the result for the *d*-spacing of the polymer. Notably, the CO_2 and CH_4 permeabilities increase from **6FDA-DH** to **6FDA-MH** because of the enhancement of both gas diffusivity and solubility. In addition, the solubility values of CO_2 and CH_4 for **6FDA-FH** are approximately 1.06 and 2.13 times higher than that of **6FDA-DH**, respectively. This is because **6FDA-DH** contains a tertiary amine in the pyridine unit, which causes strongly CO_2 affinity and increased CO_2 solubility.

According to the solution-diffusion mechanism for gas separation, the gas selectivity of glassy polymers is governed by the gas diffusion selectivity (α_D) and solubility selectivity (α_S).[28] As shown in Table 5, the separation performance of CO_2/CH_4 for the three PI membranes is mainly determined by α_S. However, the α_S of CO_2/CH_4 is approximately 1.67 times higher than α_D in **6FDA-FH**, and the α_S of CO_2/CH_4 is 6.21 and 3.95 times higher than α_D in **6FDA-DH** and **6FDA-MH**, respectively. This is because the CO_2 molecule has strong C=O dipole bonds and has a quadrupole moment; therefore, the introduction of a polarisable pyridine unit can enhance the CO_2 affinity of the polymer.[49] Hence, the presence of the polymer with the pyridine group accelerated the adsorption rate and decelerated the desorption rate of CO_2, resulting in the diffusion degradation of CO_2 in **6FDA-DH** and **6FDA-MH**. At the same time, it is notable that the $-CH_3$ group of **6FDA-MH** disrupts the packing of polymer chains and increases the FFV, enhancing the diffusivity and solubility of CO_2 relative to those of **6FDA-DH**. Furthermore, the α_S of CO_2/CH_4 did not increase with increased CO_2 solubility in **6FDA-MH** compared with that in **6FDA-DH**; this is due to the significant improvement of CH_4 solubility exhibited by **6FDA-MH**. The results suggest that the enhancement of the CO_2/CH_4 separation performance is ascribed to the higher α_S of CO_2/CH_4 in **6FDA-DH** than that in **6FDA-FH**, and the contribution of α_D is relatively small.

4. Conclusions

In this work, three spirobichroman-based PIs (**6FDA-FH**, **6FDA-DH**, and **6FDA-MH**) with different substituent units were successfully synthesised by reacting spirobichroman-based diamines with 6FDA. These polymers had high molecular weights and exhibited excellent thermal stability and good solubility in common organic solvents. The gas permeability of **6FDA-FH** was higher than that of **6FDA-DH** because of the relatively loose chain packing arising from the relatively large dihedral angle between the plane of the substituted benzene ring and that of the adjacent benzene ring in **6FDA-FH**. The $-CH_3$ group could enhance the gas permeability of **6FDA-MH** by disrupting the packing of the chain, but has a small effect on the dihedral angle between the adjacent planes. Based on the solution-diffusion mechanism of gas separation, the membrane of **6FDA-DH** with a pyridine unit exhibited enhanced CO_2/CH_4 ($\alpha_{CO_2/CH_4} = 42$) separation performance than the membrane of
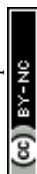
6FDA-FH with benzene. This was attributed to the presence of the polarisable pyridine unit, which enhanced the CO_2 affinity of **6FDA-DH** and improved the CO_2/CH_4 solubility selectivity. Overall, a systematic study of the relationships among the different substituents and the gas separation performance of the polymers membranes was conducted, demonstrating the critical role of the substituents for the enhancement of the gas separation performance of polymer membranes.

Conflicts of interest

There are no conflicts to declare.

References

1 T. Graham, *Philos. Trans. R. Soc. London*, 1866, **156**, 399–439.
2 P. F. Zito, A. Brunetti, E. Drioli and G. Barbieri, *Ind. Eng. Chem. Res.*, 2020, **59**, 7054–7060.
3 M. Wang, Z. Wang, S. Zhou, J. Wang, S. Liu, S. Wei, W. Guo and X. Lu, *Appl. Surf. Sci.*, 2020, **506**, 144675.
4 Z. X. Low, P. M. Budd, N. B. McKeown and D. A. Patterson, *Chem. Rev.*, 2018, **118**, 5871–5911.
5 L. M. Robeson, *J. Membr. Sci.*, 1991, **61**, 165–185.
6 L. M. Robeson, *J. Membr. Sci.*, 2008, **320**, 390–400.
7 M. Carta, R. Malpass-Evans, M. Croad, Y. Rogan, J. C. Jansen, P. Bernardo, F. Bazzarelli and N. B. McKeown, *Science*, 2013, **339**, 303–307.
8 M. Carta, M. Croad, R. Malpass-Evans, J. C. Jansen, P. Bernardo, G. Clarizia, K. Friess, M. Lanc and N. B. McKeown, *Adv. Mater.*, 2014, **26**, 3526–3531.
9 Y. Rogan, L. Starannikova, V. Ryzhikh, Y. Yampolskii, P. Bernardo, F. Bazzarelli, J. C. Jansen and N. B. McKeown, *Polym. Chem.*, 2013, **4**, 3813–3820.
10 X. Ma, B. Ghanem, O. Salines, E. Litwiller and I. Pinnau, *ACS Macro Lett.*, 2015, **4**, 231–235.
11 B. S. Ghanem, R. Swaidan, E. Litwiller and I. Pinnau, *Adv. Mater.*, 2014, **26**, 3688–3692.
12 M. A. Abdulhamid, G. Genduso, Y. Wang, X. Ma and I. Pinnau, *Ind. Eng. Chem. Res.*, 2020, **59**, 5247–5256.
13 D. Meis, A. Tena, S. Neumann, P. Georgopanos, T. Emmler, S. Shishatskiy, S. Rangou, V. Filiz and V. Abetz, *Polym. Chem.*, 2018, **9**, 3987–3999.
14 S. Li, H. J. Jo, S. H. Han, C. H. Park, S. Kim, P. M. Budd and Y. M. Lee, *J. Membr. Sci.*, 2013, **434**, 137–147.
15 B. S. Ghanem, N. B. McKeown, P. M. Budd, J. D. Selbie and D. Fritsch, *Adv. Mater.*, 2008, **20**, 2766–2771.
16 X. Ma, R. Swaidan, Y. Belmabkhout, Y. Zhu, E. Litwiller, M. Jouiad, I. Pinnau and Y. Han, *Macromolecules*, 2012, **45**, 3841–3849.
17 S. Yi, X. Ma, I. Pinnau and W. J. Koros, *J. Mater. Chem. A*, 2015, **3**, 22794–22806.
18 R. Swaidan, X. Ma, E. Litwiller and I. Pinnau, *J. Membr. Sci.*, 2013, **447**, 387–394.
19 T. Corrado and R. Guo, *Mol. Syst. Des. Eng.*, 2020, **5**, 22–48.
20 Z. Wang, D. Wang and F. Zhan, *ACS Macro Lett.*, 2014, **3**, 597–601.

21 S. Wang, S. Jin, X. Han, L. Li, X. Zhao, H. Zhou and C. Chen, *Mater. Des.*, 2020, **194**, 108933.

22 C. Zhang, P. Li and B. Cao, *J. Membr. Sci.*, 2017, **530**, 176–184.

23 A. Tena, R. Vazquez-Guillo, A. Marcos-Fernandez, A. Hernandez and R. Mallavia, *RSC Adv.*, 2015, **5**, 41497–41505.

24 M. R. de la Viuda, A. Tena, S. Neumann, S. Willruth, V. Filiza and V. Abetz, *Polym. Chem.*, 2018, **9**, 4007–4016.

25 S. Wang, S. Ma, H. He, W. Ai, D. Wang, X. Zhao and C. Chen, *Polymer*, 2019, **168**, 199–208.

26 Z. Wang, D. Wang and J. Jin, *Macromolecules*, 2014, **47**, 7477–7483.

27 J. Y. Park and D. R. Paul, *J. Membr. Sci.*, 1997, **125**, 23–39.

28 C. G. Bezzu, M. Carta, A. Tonkins, J. C. Jansen, P. Bernardo, F. Bazzarelli and N. B. McKeown, *Adv. Mater.*, 2012, **24**, 5930–5933.

29 K. S. Chang, K. L. Tung, Y. F. Lin and H. Y. Lin, *RSC Adv.*, 2013, **3**, 10403–10413.

30 R. Swaidan, M. Al-Saeedi, B. Ghanem, E. Litwiller and I. Pinnau, *Macromolecules*, 2014, **47**, 5104–5114.

31 N. K. Sini, M. Azechi and T. Endo, *Macromolecules*, 2015, **48**, 7466–7472.

32 P. C. Tan, B. S. Ooi, A. L. Ahmad and S. C. Low, *J. Appl. Polym. Sci.*, 2018, **46073**, 1–11.

33 Y. Tsai, C. H. Fan, C. Y. Hung and F. J. Tsai, *Eur. Polym. J.*, 2009, **45**, 115–122.

34 Z. Mi, S. Wang, Z. Hou, Z. Liu, S. Jin, X. Wang, D. Wang, X. Zhao, Y. Zhang, H. Zhou and C. Chen, *Polymers*, 2019, **11**, 854.

35 M. A. Abdulhamid, X. Ma, X. Mia and I. Pinnau, *Polymer*, 2017, **130**, 182–190.

36 W. C. Tsen, C. F. Lee, Y. R. Su, J. H. Gu and M. C. Suen, *J. Appl. Polym. Sci.*, 2019, **136**, 47356.

37 Y. Zhuang, J. G. Seong, Y. S. Do, H. J. Jo, Z. Cui, J. Lee, Y. M. Lee and M. D. Guiver, *Macromolecules*, 2014, **47**, 3254–3262.

38 S. Wang, S. Ma, H. He, W. Ai, D. Wang, X. Zhao and C. Chen, *Polymer*, 2019, **168**, 199–208.

39 S. Wang, S. Jin, C. Wang, L. Li, X. Zhao and C. Chen, *Int. J. Energy Res.*, 2020, **44**, 1986–1998.

40 Z. Mi, Z. Liu, C. Tian, X. Zhao, H. Zhou, D. Wang and C. Chen, *J. Polym. Sci., Part A: Polym. Chem.*, 2017, **55**, 3253–3265.

41 A. Fakhar, M. Sadeghi, M. Dinari and R. Lammertink, *J. Membr. Sci.*, 2019, **574**, 136–146.

42 Y. R. Chen, L. H. Chen, K. S. Chang, T. H. Chen, Y. F. Lin and K. L. Tung, *J. Membr. Sci.*, 2016, **514**, 114–124.

43 D. Hofmann, M. Entrialgo-Castano, A. Lerbret, M. Heuchel and Y. Yampolskii, *Macromolecules*, 2003, **36**, 8528–8538.

44 K. S. Chang, Y. H. Huang, K. R. Lee and K. L. Tung, *J. Membr. Sci.*, 2010, **354**, 93–100.

45 K. S. Chang, C. C. Tung, K. S. Wang and K. L. Tung, *J. Phys. Chem. B*, 2009, **113**, 9821–9830.

46 Z. Wang, A. P. Isfahani, K. Wakimoto, B. B. Shrestha, D. Yamaguchi, B. Ghalei and E. Sivaniah, *ChemSusChem*, 2018, **11**, 2744–2751.

47 A. X. Wu, J. A. Drayton, K. M. Rodriguez, Q. i. Qian, S. Lin and Z. P. Smith, *Macromolecules*, 2020, **53**, 5085–5095.

48 G. Deng, Y. Wang, X. Zong, X. Yuan, J. Luo, X. Wang and S. Xue, *Polymer*, 2019, **183**, 121854.

49 C. H. Jung and Y. M. Lee, *Macromol. Res.*, 2008, **16**, 555–560.